

## Article

# On Grain Boundary Engineering for a 316L Austenitic Stainless Steel

Pavel Dolzhenko, Marina Tikhonova, Marina Odnobokova , Rustam Kaibyshev and Andrey Belyakov \* 

Laboratory of Mechanical Properties of Nanostructured Materials and Superalloys, Belgorod State University, 308015 Belgorod, Russia

\* Correspondence: belyakov@bsu.edu.ru

**Abstract:** The change in the grain boundary network during recrystallization and grain growth was studied in a 316L austenitic stainless steel subjected to 5% cold rolling reduction. The primary recrystallization rapidly developed upon heating to 1000 °C, resulting in the development of relatively coarse-grained microstructure with a grain size about 100 μm. The recrystallized microstructures contained large fractions of annealing twins with their  $\Sigma^{3^n}$  SCL boundaries. The latter ones served as interrupters of the ordinary grain boundary network. The fraction of  $\Sigma^{3^n}$  CSL boundaries increased with increasing the grain size during prolonged annealing. On the other hand, the number of interruptions per unit area remained nearly the same during annealing. Hence, the number of interruptions per a grain increased in accordance with a power law function of the grain size with an exponent of 2. The relationships obtained for the grain boundary network evolution can be used to predict the microstructure evolution in austenitic stainless steels during primary recrystallization followed by grain growth.

**Keywords:** austenitic stainless steel; grain boundary engineering; primary recrystallization; annealing twins; grain boundary interruption



**Citation:** Dolzhenko, P.; Tikhonova, M.; Odnobokova, M.; Kaibyshev, R.; Belyakov, A. On Grain Boundary Engineering for a 316L Austenitic Stainless Steel. *Metals* **2022**, *12*, 2185. <https://doi.org/10.3390/met12122185>

Academic Editor: Frank Czerwinski

Received: 3 December 2022

Accepted: 15 December 2022

Published: 19 December 2022

**Publisher's Note:** MDPI stays neutral with regard to jurisdictional claims in published maps and institutional affiliations.



**Copyright:** © 2022 by the authors. Licensee MDPI, Basel, Switzerland. This article is an open access article distributed under the terms and conditions of the Creative Commons Attribution (CC BY) license (<https://creativecommons.org/licenses/by/4.0/>).

## 1. Introduction

Mechanical and physical properties of polycrystalline metals and alloys depend significantly on their microstructures, in which the boundaries between the crystallites play an important role [1,2]. The grain boundaries affect the dislocation motion and, therefore, control the strength, plasticity, fracture, etc. [3–5]. Moreover, the internal distortions of grain boundaries determine the diffusivity and influence the rate of diffusion-controlled processes, e.g., intercrystalline corrosion [6–8].

An approach aimed at the development of desired grain boundary ensemble has been specified as grain boundary engineering [9]. One promising application of grain boundary engineering deals with improving the intergranular corrosion resistance of austenitic stainless steels [10]. This approach involves the optimization of grain boundary character distribution in order to increase the fraction of so-called special boundaries with a high density of coincident site lattice (CSL), i.e.,  $\Sigma^{3^n}$  CSL twin boundaries, that are characterized by a relatively low energy, thus slowing down the diffusion rate. Correspondingly, the aim of grain boundary engineering is to interrupt the connectivity of ordinary grain boundary network by  $\Sigma^{3^n}$  CSL boundaries as much as possible [11,12]. The development of  $\Sigma^{3^n}$  CSL boundaries in austenitic stainless steels with low stacking fault energy (SFE) is associated with annealing twins appearing during recrystallization and grain growth [13–15]. The studies dealing with grain boundary engineering in austenitic stainless steels are focused on the fraction and density of  $\Sigma^{3^n}$  CSL boundaries. Pande et al. showed that the density of annealing twins ( $\rho_{\text{CSL}}$ ) can be expressed by a unique function of the grain size ( $D$ ), i.e.,  $\rho_{\text{CSL}} \sim D^{-1} \log D$  [13]. By studying the recrystallization and grain growth behavior in austenitic steels with ultrafine grains evolved by severe plastic deformation, Tikhonova

and Odnobokova et al. defined the fraction of  $\Sigma 3^n$  CSL boundaries and their density as functions of a ratio of the annealed grain size to initial one [16,17]. The obtained relationships predict a rapid increase in the fraction of  $\Sigma 3^n$  CSL boundaries at an early stage of recrystallization, followed by slowing down the rate of increase upon further grain growth, as is frequently observed in experiments [18,19]. Similarly, following the rapid rise at the beginning of recrystallization, the density of  $\Sigma 3^n$  CSL boundaries gradually decreases during subsequent grain growth. Therefore, a large fraction of  $\Sigma 3^n$  CSL boundaries in austenitic stainless steels could be expected after rapid grain nucleation/growth, owing to primary recrystallization. Fang et al. showed the development of large grain clusters, in which the grains are interfaced by  $\Sigma 3^n$  CSL boundaries during annealing following a small cold strain (about 5% rolling reduction) [20]. However, the regularities of the disruption of the random grain boundary network by  $\Sigma 3^n$  CSL boundaries have not been clarified. The effect of annealing twin formation during recrystallization and grain growth on the interruption of grain boundaries of general type has not been studied in sufficient detail. A lack of experimental studies on the quantitative analysis of the grain boundary interruptions makes it difficult to develop constitutive relationships for grain boundary engineering of austenitic stainless steels.

Therefore, the present study aims to compensate for a deficiency in experimental results for the relationships between the recrystallization/grain growth, the fraction of  $\Sigma 3^n$  CSL boundaries, and the disruption of random grain boundary network. In particular, the present paper considers the change in the number density of grain boundary interruptions in cold worked 316L-type stainless steel subjected to recrystallization annealing.

## 2. Materials and Methods

A hot forged 316L-type austenitic stainless steel, Fe-0.04%C-17.3%Cr-10.7%Ni-1.7%Mn-2%Mo-0.4%Si-0.04%P-0.05%S (all in wt.%), was used as the starting material. An initial annealing at 1100 °C for an hour resulted in the uniform equiaxed microstructure with an average grain size of 90  $\mu\text{m}$  and the fraction of  $\Sigma 3^n$  CSL boundaries of 0.54. Then, the steel samples with a thickness of about 2 mm were cold rolled with a 5% rolling reduction at ambient temperature and annealed in air at 700–1100 °C for 5 min to 50 h using conventional muffle furnace.

Annealing softening was studied by means of the Vickers hardness test with a load of 2 N. The structural investigations were carried out on the sample sections perpendicular to the transverse direction (TD) using a Quanta 600 scanning electron microscope (FEI, Hillsboro, OR, USA) (SEM) equipped with an electron back-scattered diffraction (EBSD) detector incorporating orientation imaging microscopy (OIM) with TSL OIM Analysis 6 software (EDAX, Inc., Mahwah, NJ, USA). The specimens for EBSD were electro-polished using an electrolyte containing 10% perchloric acid and 90% acetic acid at a voltage of 20 V at room temperature. The OIM micrographs for approx. 1 mm<sup>2</sup> areas of observation were obtained with a step size of 1  $\mu\text{m}$ . The recrystallization progress was analyzed by means of the grain orientation spread (GOS) values, setting the grain tolerance angle of 5°. The grain size was measured by a linear intercept method as a spacing of high-angle boundaries with a misorientation of  $\theta \geq 15^\circ$ , omitting  $\Sigma 3^n$  CSL boundaries. The latter ones were defined using Brandon's criterion ( $15^\circ / \Sigma^{0.5}$ ). The distributions of the boundary/sub-boundary triple junctions were obtained by counting at least 100 junctions.

## 3. Results

### 3.1. Annealed Microstructures

Typical microstructures developed in a 316L stainless steel after cold rolling followed by isochronal annealing for 1 h at 700–1100 °C are shown in Figure 1 as maps of grain orientation spread. In spite of quite a small cold strain (rolling reduction of 5%), the cold worked steel sample is characterized by large GOS values. Most of the grains experience orientation spread over 2–4° (Figure 1a). Subsequent annealing at temperatures of 700–900 °C leads to a partial release of the internal distortions. As a result, the grain orientation spread in the range of 1–2°

is observed in the grains in Figure 1b–d. Hence, it can be concluded that static recovery takes place in the present cold rolled steel samples during annealing at 700–900 °C.

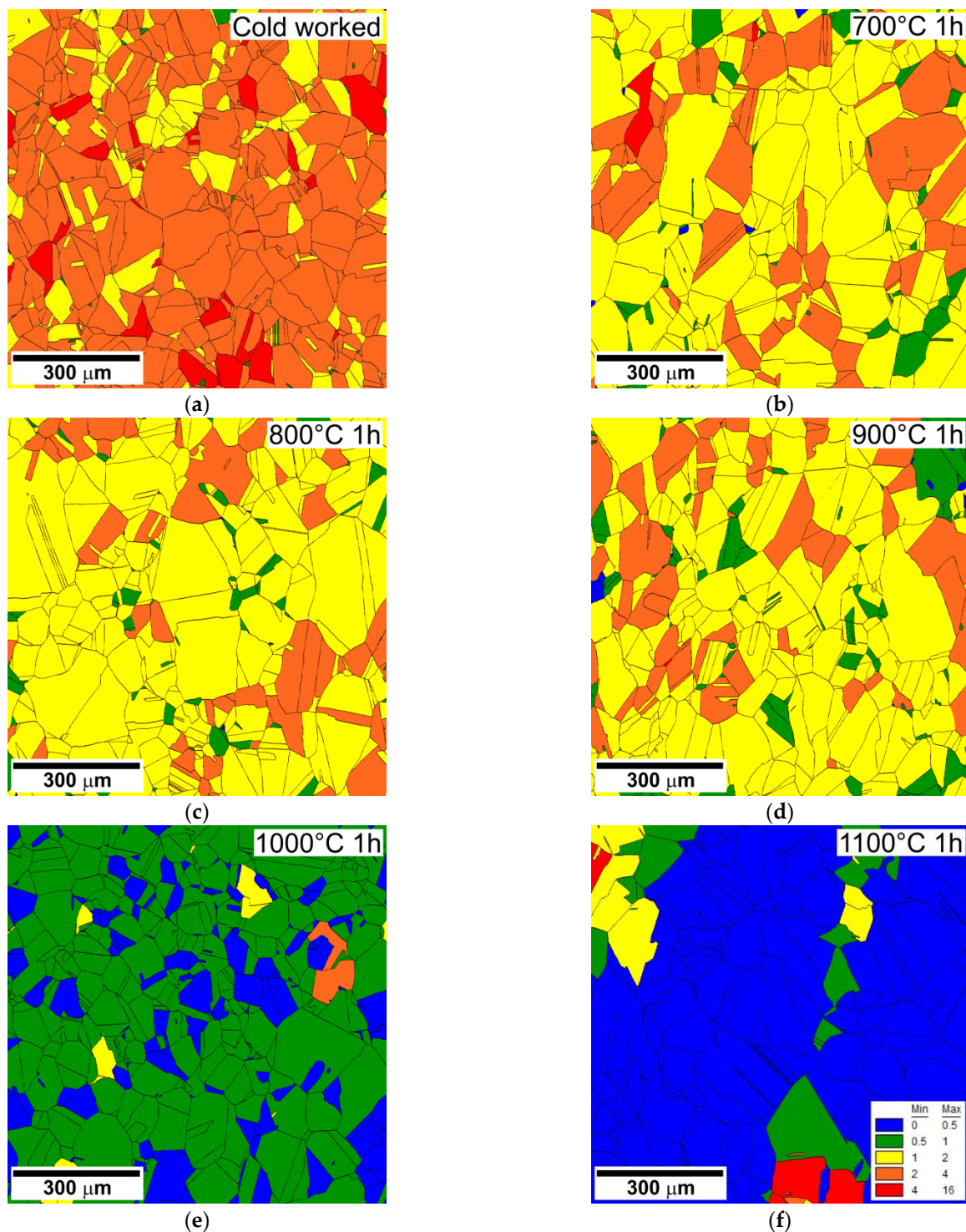


**Figure 1.** Grain orientation spread in the steel samples subjected to cold rolling with 5% reduction (a), and then annealed for 1 h at 700 °C (b), 800 °C (c), 900 °C (d), 1000 °C (e), and 1100 °C (f). The colour correspondence is shown in the inset in (f).

On the other hand, annealing at temperatures of  $T \geq 1000$  °C results in complete softening of the cold rolled samples. Almost all grains in the microstructures annealed at 1000 °C and 1100 °C are characterized by GOS below 1° (Figure 1e,f). Note here that some

grains with relatively large GOS values appear in Figure 1e,f because of their low-angle sub-boundaries. The latter ones can be present even in well annealed microstructures and formally increase the grain orientation spread as calculated by OIM analysis. Taking the grains with GOS below  $1^\circ$  as the recrystallized grains, the recrystallized fraction is plotted in Figure 2 versus temperature of annealing. The hardness of annealed samples is also indicated in Figure 2. It is clearly seen in Figure 2 that the hardness gradually decreases with increasing temperature due to promoted recovery followed by recrystallization. In contrast, by selecting the recrystallized grains based on their GOS values, the primary static recrystallization development is clearly distinguished in the present cold rolled steel samples during annealing at 1000–1100 °C.

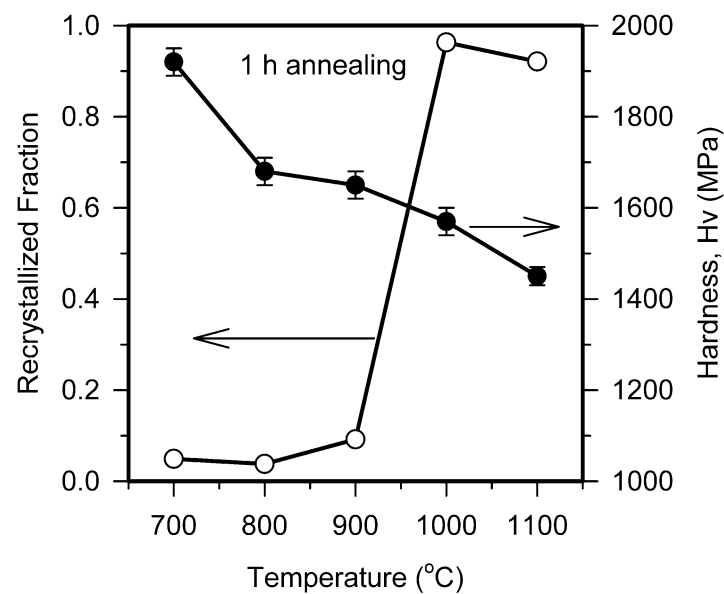


**Figure 2.** Recrystallized fraction calculated as the area fraction of grains with grain orientation spread below  $1^\circ$  and the hardness of the steel samples subjected to 5% cold rolling reduction followed by 1 h of annealing.

The grain boundary misorientation distributions developed in the annealed microstructures are shown in Figure 3 for the misorientation range of  $2^\circ$  to  $64^\circ$ . Two sharp peaks stand out against small (below  $4^\circ$ ) and large (around  $60^\circ$ ) misorientations of the cold rolled microstructure. The small misorientations correspond to numerous low-angle dislocation sub-boundaries evolved by plastic deformation. On the other hand, the large misorientations are associated with twin boundaries that are essentially  $\Sigma 3^n$  CSL boundaries that can be represented by  $60^\circ$  rotations around  $\langle 111 \rangle$ . Evidently, cold rolling with quite a small rolling reduction of 5% did not disturb the specific crystallographic orientation of original annealing twins. All the grain boundary misorientation distributions among the annealed microstructures are characterized by sharp peaks for  $60^\circ$  misorientations. In the recovered microstructures, the twin boundaries remained the twins of the original microstructure. Recovery annealing is accompanied by a decrease in the dislocation density and the corresponding fraction of low-angle dislocation sub-boundaries, while the high-angle grain boundary characters are not affected remarkably. In contrast, the large fractions of  $\Sigma 3^n$  CSL boundaries in the recrystallized microstructures result from the annealing twins evolved by the present primary recrystallization. Grain boundary engineering in austenitic stainless steels deals with annealing twin formation that is closely connected with recrystallization and grain growth. Therefore, the samples annealed at 1000–1100 °C will be selected for further detailed analysis.

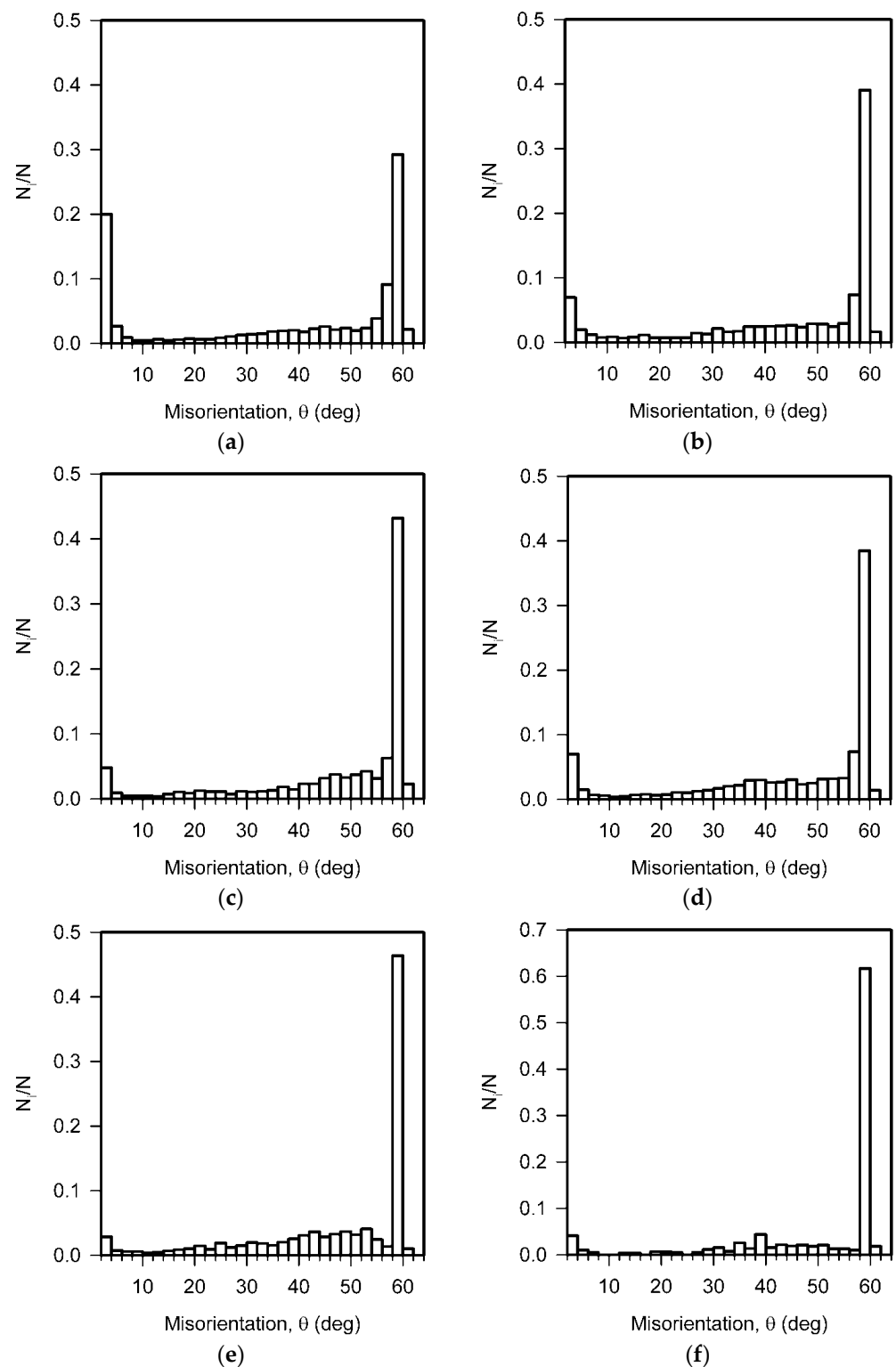


**Figure 3.** Grain boundary misorientation distribution in the steel samples subjected to cold rolling with 5% reduction (a), and then annealed for 1 h at 700 °C (b), 800 °C (c), 900 °C (d), 1000 °C (e), and 1100 °C (f).

### 3.2. Grain Boundary Interruption

Representative images of the microstructures evolved during annealing at 1000 °C and 1100 °C are shown in Figure 4, which displays the grain boundary networks selecting the ordinary grain boundaries and the  $\Sigma 3^n$  CSL boundaries by black and red colors,

respectively. Increasing both the temperature and time for recrystallization annealing results in an increase in the recrystallized grain size. The number of annealing twins per unit area apparently decreases as the grain size increases during recrystallization. However, the fraction of the twin boundaries increases with an increase in annealing time. Moreover, many uncompleted ordinary grain boundaries are clearly seen in Figure 4 (some of them are indicated by the black arrows). These uncompleted boundaries are frequently interrupted by  $\Sigma 3^n$  CSL boundaries. Therefore, the recrystallization/grain growth results in the development of the disrupted grain boundary network.

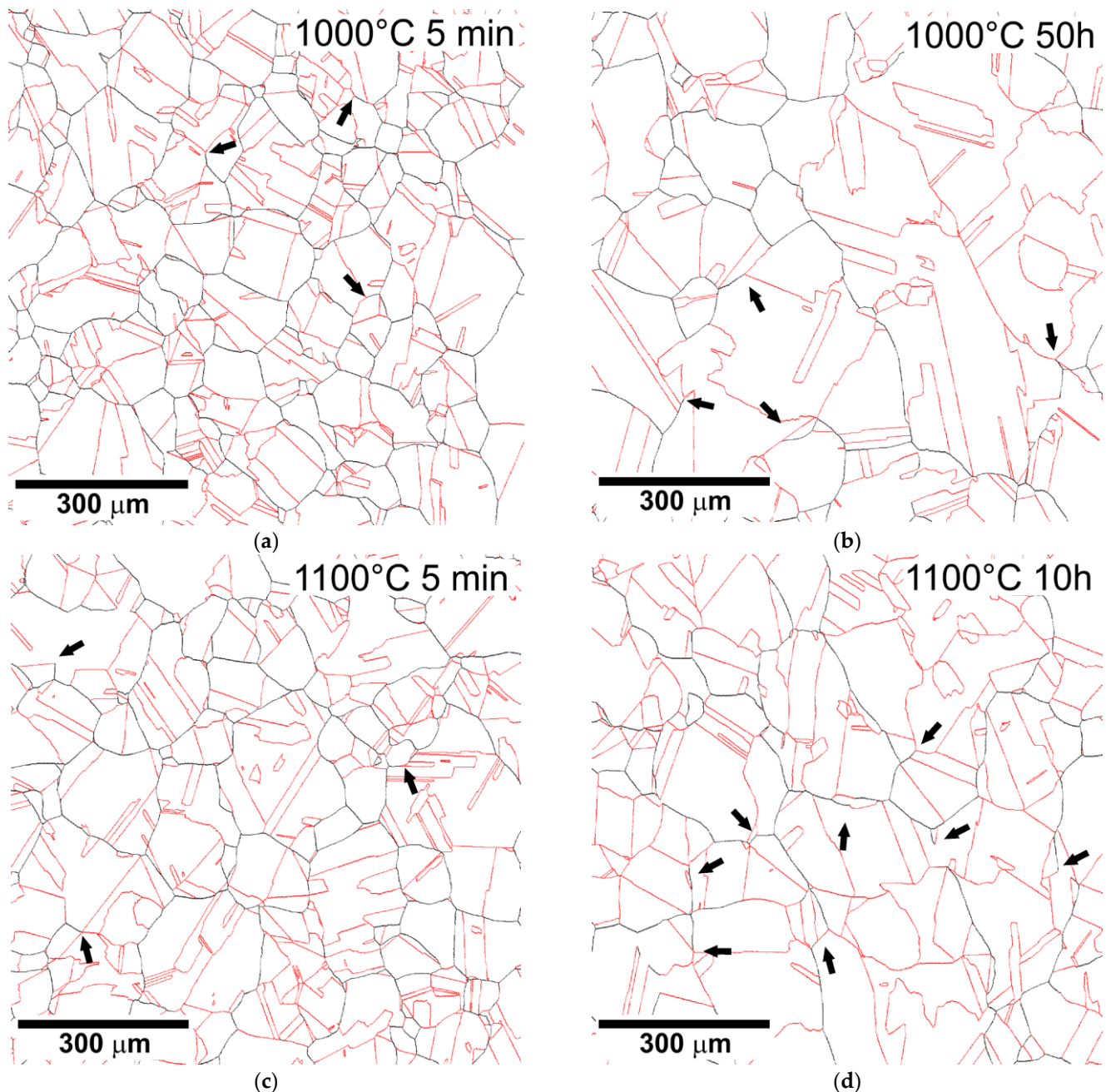


**Figure 4.** Grain boundary network in the steel samples annealed at 1000 °C for 5 min (a), at 1000 °C for 50 h (b), at 1100 °C for 5 min (c), and at 1100 °C for 10 h (d). Black and red lines indicate ordinary and  $\Sigma 3^n$  CSL boundaries, respectively.

The grain growth kinetics is illustrated in Figure 5a. The grain size is about 100–150 μm as developed by the primary recrystallization after short time annealing, and an increase in

annealing temperature leads to a coarser microstructure. A remarkable increase in the grain size is observed after annealing for about 10 h, when the grain size attains 200–250  $\mu\text{m}$ . Note here that the temperature effect on the recrystallized grain size diminishes with increasing annealing time. Commonly, the size of grains evolved by primary recrystallization increases with a decrease in the preceding cold strain [10]. The small cold rolling strain used in the present study leads to the evolution of large, recrystallized grains that, in turn, impairs the analysis of the grain growth behavior. Nevertheless, assuming a power law relationship for normal grain growth in Figure 5a, the present data can be roughly expressed with a grain growth exponent of approx. 8, similar to other studies on the grain growth in austenitic stainless steels [21].

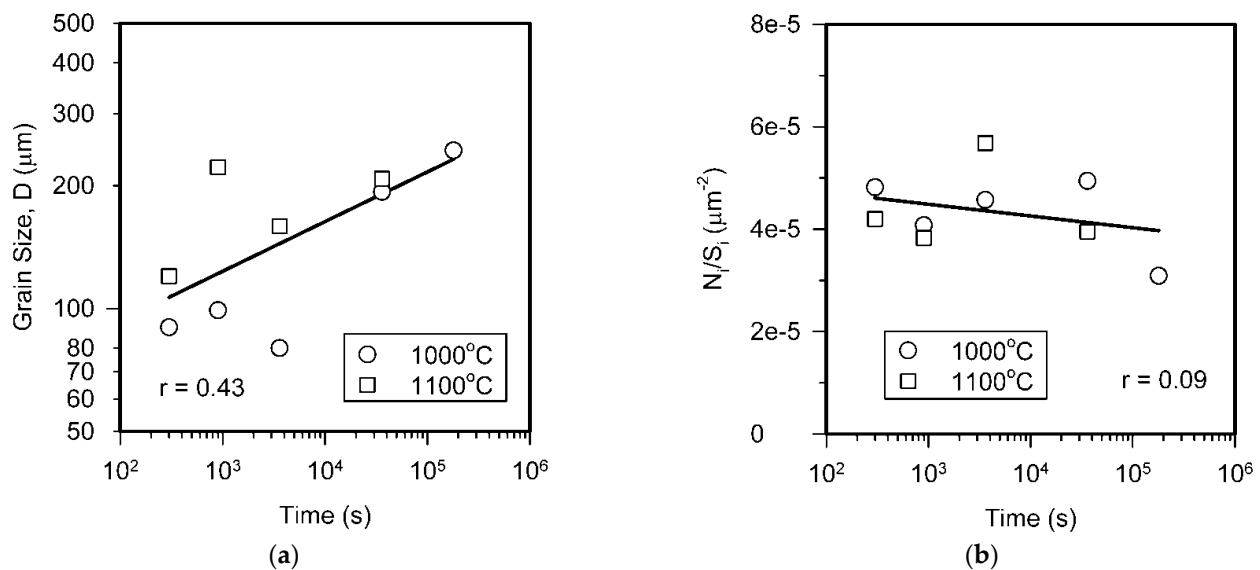


**Figure 5.** Effect of annealing time on the grain size (a) and the number of grain boundary interruptions per unite area (b) for a 316L stainless steel subjected to recrystallization annealing followed by grain growth. The values of the determination coefficient ( $r$ ) correspond to the linear regressions.

In contrast, the density of the interruptions of ordinary grain boundaries by  $\Sigma 3^n$  CSL boundaries is almost independent of annealing time. Figure 5b shows the change in the number of interruptions per unit area during annealing. About  $4 \times 10^{-5}$  interruptions per sq. micrometer are observed in the samples irrespective of annealing duration. Such time invariant interruption density suggests that the disruption of the grain boundary network occurs at early annealing, i.e., at the beginning stage of primary recrystallization. It should be noted that the appearance of numerous annealing twins has also been attributed to the early recrystallization stage, which is characterized by rapid grain boundary motion [13,16,18].

The evolution of the grain boundary ensemble should be reflected by the change in the distribution of grain boundary junctions. Specific grain boundary junctions consist of three ordinary grain boundaries (J3), two ordinary grain boundaries and one special boundary (J2), one ordinary grain boundary and two special boundaries (J1), and three special boundaries (J0). Figure 6 shows the change in the fractions of triple junctions composed of different boundaries, J3–J0, with temperature compensated annealing time,  $t^* = t \exp(-Q/RT)$ , where  $t$  is annealing time,  $Q$  is the activation energy for grain boundary diffusion (167 kJ/mol [22]),  $R$  is the universal gas constant, and  $T$  is the temperature [23]. The fraction of J3 junctions of about 0.2 is relatively small and tends to slightly decrease with increasing annealing time. The J2 junctions compose the largest fraction of about 0.6 after short annealing time. An increase in annealing time leads to a significant decrease in the J2 fraction below 0.4 in Figure 6b. It is interesting to note that the J1 junctions compose a small fraction of approx. 0.1, irrespective of annealing time (Figure 6c). This is consistent with quite a weak time dependence of the number density of grain boundary interruptions

in Figure 5b. In contrast, the J0 fraction in Figure 6d remarkably increases from about 0.2 to 0.6 with an increase in annealing time. Increasing the J0 fraction reflects an increase in the fraction of  $\Sigma 3^n$  CSL boundaries during recrystallization/grain growth. Almost the same evolution of the fraction of each type of triple junctions has been obtained by mesoscale Monte Carlo modelling [24].

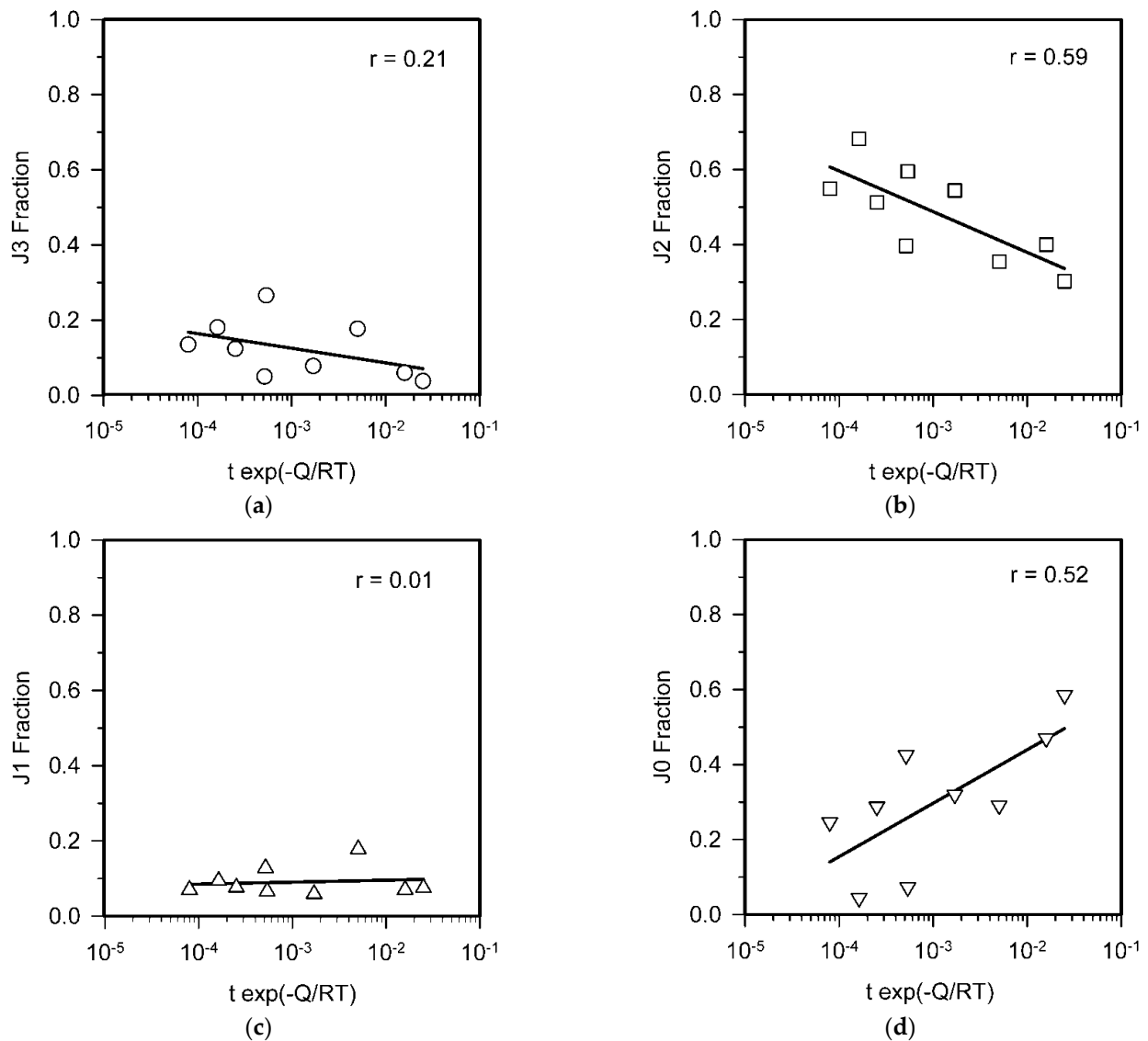


**Figure 6.** Effect of the temperature compensated annealing time on the fraction of triple junctions composed of three ordinary grain boundaries (a); two ordinary grain boundaries and one special boundary (b); one ordinary grain boundary and two special boundaries (c); and three special boundaries (d). The values of the determination coefficient (r) correspond to the linear regressions.

#### 4. Discussion

Assuming that the twin appearance depends on the boundary migration velocity, the fraction of  $\Sigma 3^n$  CSL boundaries,  $F_{CSL}$ , is expressed by the grain size increase ( $D/D_0$ ), where  $D$  is the annealed grain size and  $D_0$  is the initial one, i.e., just before grain growth started) [16]:

$$F_{CSL} = (N_{CSL0} + K \ln(D/D_0)) / (1 + N_{CSL0} + K \ln(D/D_0)) \quad (1)$$

Here,  $K$  is a numerical factor varying from 0 upward,  $N_{CSL0}$  is the number of twin-related boundaries in an initial grain, and  $F_{CSL0}$  is the initial fraction of  $\Sigma 3^n$  CSL boundaries (before grain growth). In the present study,  $N_{CSL0}$  can be taken as zero, because primary

recrystallization should completely replace the initial microstructure. Then, the following relationship can be obtained:

$$(F_{\text{CSL}}^{-1} - 1)^{-1} = K \ln D - K \ln D_0 \quad (2)$$

The relationship between  $(F_{\text{CSL}}^{-1} - 1)^{-1}$  and  $D$  is represented in Figure 7a. The numerical factors of  $K = 1.4$  and  $D_0 = 35 \mu\text{m}$  can be obtained for  $1000^\circ\text{C}$  annealing and those of  $K = 2.6$  and  $D_0 = 61 \mu\text{m}$  for  $1100^\circ\text{C}$  annealing. The larger  $K$  value corresponds to the higher probability of twin formation at higher annealing temperature, and  $D_0$  can be considered as a grain size just developed by primary recrystallization that should also be larger at higher annealing temperature.

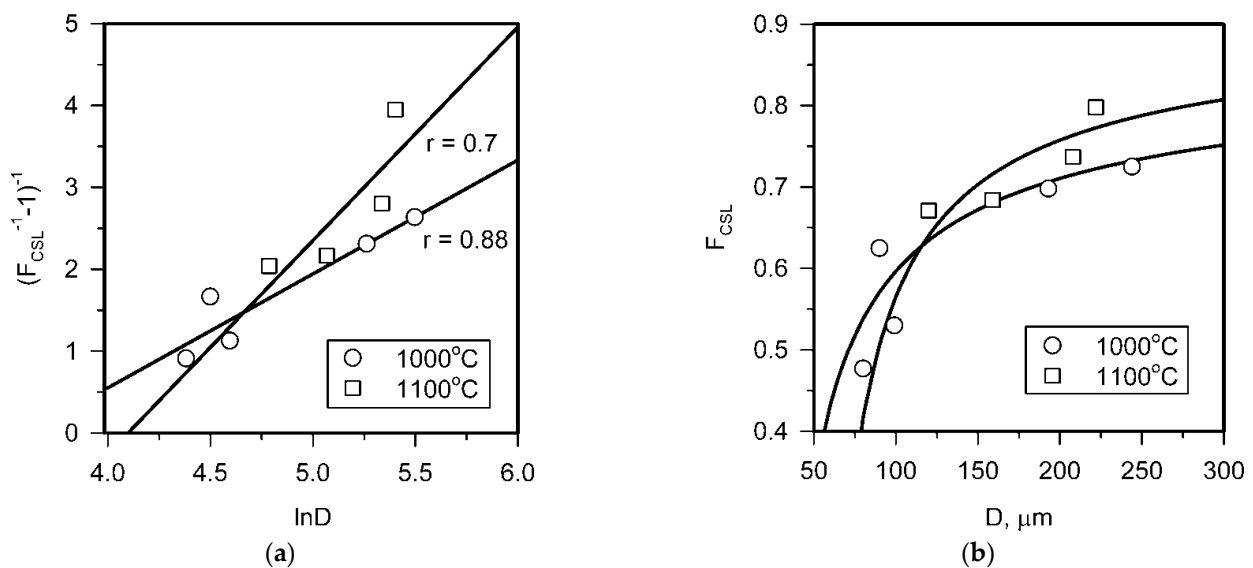


**Figure 7.** Change in the  $\Sigma 3^n$  CSL boundary fraction ( $F_{\text{CSL}}$ ) with increasing the grain size ( $D$ ) shown as plots of  $(F_{\text{CSL}}^{-1} - 1)^{-1}$  vs.  $\ln D$  (a) and  $F_{\text{CSL}}$  vs.  $D$  (b) in a 316L stainless steel subjected to recrystallization annealing followed by grain growth.

The fraction of  $\Sigma 3^n$  CSL boundaries as calculated by Equation (1) using the obtained parameters of  $K$  and  $D_0$  is represented by solid lines in Figure 7b along with experimental data (open symbols). It is clearly seen in Figure 7b that the grain growth is accompanied by an increase in the fraction of  $\Sigma 3^n$  CSL boundaries. The rapid increase in the fraction of  $\Sigma 3^n$  CSL boundaries occurs at the beginning of grain growth, when  $F_{\text{CSL}}$  increases well above 0.6. Then, the rate of increase in  $F_{\text{CSL}}$  decreases upon further annealing that leads  $F_{\text{CSL}}$  to approach 0.8 after long time treatment. This is consistent with previous studies on the grain boundary engineering of ultrafine grained stainless steels subjected to severe plastic deformation [16,17].

It has been suggested that the triple junctions can drag the boundary motion, or vice versa, and their role and properties should be taken into consideration while discussing the grain growth [25]. The change in the fraction of different grain boundary junctions during annealing (Figure 6) should be associated with their mobility. Namely, the number fraction of the most mobile junctions is expected to decrease during the grain coarsening, whereas that of the stable junctions should increase. Thus, the junction mobility can be discussed as follows.

J3: The triple junctions of ordinary grain boundaries should be characterized by moderate mobility. The motion of J3 junctions depends on their proximity to equilibrium state, e.g., equilibrium angles of  $120^\circ$ , etc. Therefore, the J3 fraction slightly decreases during grain growth (Figure 6a).

J2: The mobility of joining two ordinary grain boundaries with one special boundary depends on the mutual arrangement of the ordinary boundaries. The high surface tension

of the latter ones should lead to high J2 mobility. As a result, the fraction of J2 junctions decreases during grain growth (Figure 6b).

J1: A nearly constant fraction of J1 junctions during grain growth (Figure 6c) suggests their limited mobility. Indeed, the special boundaries such as  $\Sigma 3^n$  twin boundaries are generally characterized by low mobility [2]. Thus, triple junctions should be rather stable in the case of two joining special boundaries.

J0: Such triple junctions consisting of three special boundaries should be the most stable ones from the viewpoint of migration ability. Low surface energy of the special boundaries is responsible for quite low mobility of J0 junctions and an increase in their fraction with grain growth during annealing (Figure 6d).

The numbers of grain boundary interruptions in Figure 5b and the J1 fraction in Figure 6c are characterized by very weak dependences on the annealing time. These relationships suggest that the grain boundary interruptions evolve at early recrystallization and remain invariable during further grain growth. Therefore, the change in the disruption of ordinary grain boundary network during annealing can be discussed only in comparison/relation to the change in other microstructural parameters. If the number of grain boundary interruptions per unit area is constant during annealing, the number of interruptions per a grain should be proportional to the square of grain size ( $D$ ), i.e.,  $N_i/N_{D_i} \sim D^2$ , where  $N_i$  is the number density of interruptions and  $N_{D_i}$  is the number of grains per unit area. The relationship between  $N_i/N_{D_i}$  and  $D$  is represented in Figure 8. It is clearly seen that the number of grain boundary interruptions per grain can be expressed by a power law function of the grain size with an exponent of 2. Therefore, the grain growth during prolonged recrystallization annealing is accompanied by progressive disruption of the ordinary grain boundary network. The long recrystallization annealing of austenitic stainless steels subjected to light cold working can be considered as a promising method of grain boundary engineering.

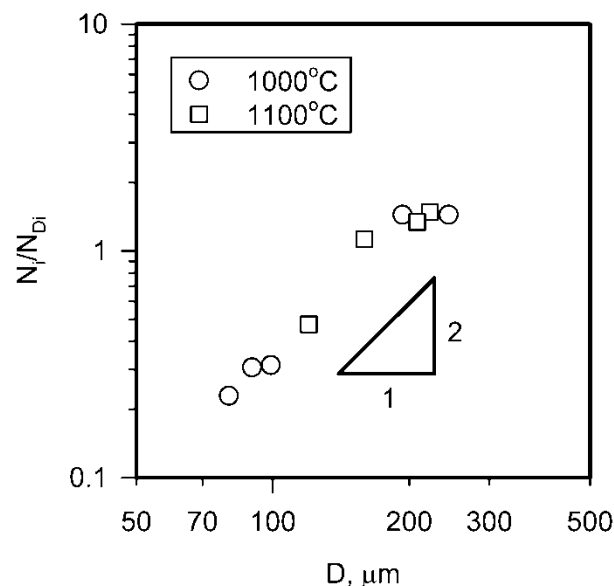


**Figure 8.** Relationship between the number of grain boundary interruptions per grain ( $N_i/N_{D_i}$ ) and the grain size ( $D$ ) in a 316L stainless steel subjected to recrystallization annealing followed by grain growth.

## 5. Conclusions

The grain boundary network evolution in a 316L austenitic stainless steel during recrystallization followed by grain growth was studied. The main conclusions can be summarized as follows.

1. The primary recrystallization readily developed during annealing at temperatures of  $T \geq 1000$  °C in the steel samples subjected to cold rolling with a reduction of 5%, resulting in the coarse-grained microstructures with a grain size of about 100  $\mu\text{m}$ .
2. The annealed microstructures were characterized by a large fraction of  $\Sigma 3^n$  CSL boundaries associated with numerous annealing twins. The fraction of these special boundaries increased with an increase in the grain size during prolonged annealing.
3. The grain growth during annealing was accompanied by an increase in the number of grain boundary interruptions per grain. The relative number of the grain boundary interruptions can be expressed by a power law function of the grain size with an exponent of 2. Small strain cold rolling followed by prolonged recrystallization annealing is suggested as an advanced method of grain boundary engineering for austenitic stainless steels.

**Author Contributions:** Conceptualization, A.B.; methodology, M.T.; software, P.D.; validation, P.D., M.T. and M.O.; formal analysis, A.B.; investigation, P.D.; writing—original draft preparation, A.B.; writing—review and editing, M.O.; supervision, R.K.; project administration, M.T.; funding acquisition, R.K. All authors have read and agreed to the published version of the manuscript.

**Funding:** This research was funded by the Russian Science Foundation, Agreement number 22-43-02012.

**Data Availability Statement:** The data presented in this study are available upon request from the corresponding author.

**Acknowledgments:** The work was carried out using the equipment of the Joint Research Center, Technology and Materials, of Belgorod National Research University.

**Conflicts of Interest:** The authors declare no conflict of interest.

## References

1. Watanabe, T. Approach to Grain Boundary Design for Strong and Ductile Polycrystals. *Res. Mech.* **1984**, *11*, 47–84.
2. Randle, V. *The Measurement of Grain Boundary Geometry*; Taylor and Francis Group: London, UK, 2017. [[CrossRef](#)]
3. Gertsman, V.Y.; Bruemmer, S.M. Study of grain boundary character along intragranular stress corrosion crack paths in austenitic alloys. *Acta Mater.* **2001**, *49*, 1589–1598. [[CrossRef](#)]
4. Watanabe, T.; Tsurekawa, S. Toughening of brittle materials by grain boundary engineering. *Mater. Sci. Eng. A* **2004**, *387–389*, 447–455. [[CrossRef](#)]
5. Kobayashi, S.; Maruyama, T.; Tsurekawa, S.; Watanabe, T. Grain boundary engineering based on fractal analysis for control of segregation-induced intergranular brittle fracture in polycrystalline nickel. *Acta Mater.* **2012**, *60*, 6200–6212. [[CrossRef](#)]
6. Palumbo, G.; Lehockey, E.M.; Lin, P. Applications for grain boundary engineered materials. *J. Miner.* **1998**, *50*, 40–43. [[CrossRef](#)]
7. Gao, X.; Wang, M.; Liu, T.; Lu, Y.; Ejaz, A. Investigation on thermo-mechanical processing and intergranular corrosion of TP347H stainless steel. *Mater. Sci. Technol.* **2021**, *37*, 909–917. [[CrossRef](#)]
8. Zhang, M.; Zhang, C.; Wu, H.; Yang, B. Effects of grain boundary engineering on the microstructure and corrosion fatigue properties of 316L austenitic stainless steel. *Front. Mater.* **2022**, *9*, 931848. [[CrossRef](#)]
9. Watanabe, T. Grain boundary engineering: Historical perspective and future prospects. *J. Mater. Sci.* **2011**, *46*, 4095–4115. [[CrossRef](#)]
10. Tsurekawa, S.; Nakamichi, S.; Watanabe, T. Correlation of grain boundary connectivity with grain boundary character distribution in austenitic stainless steel. *Acta Mater.* **2006**, *54*, 3617–3626. [[CrossRef](#)]
11. Shimada, M.; Kokawa, H.; Wang, Z.J.; Sato, Y.S.; Karibe, I. Optimization of grain boundary character distribution for intergranular corrosion resistant 304 stainless steel by twin-induced grain boundary engineering. *Acta Mater.* **2002**, *50*, 2331–2341. [[CrossRef](#)]
12. Fang, X.; Wang, W.; Cai, Z.; Qin, C.; Zhou, B. The evolution of cluster of grains with  $\Sigma 3^n$  relationship in austenitic stainless steel. *Mater. Sci. Eng. A* **2010**, *A527*, 1571–1576. [[CrossRef](#)]
13. Pande, C.S.; Imam, M.A.; Rath, B.B. Study of Annealing Twins in FCC Metals and Alloys. *Metall. Trans. A* **1990**, *21*, 2891–2896. [[CrossRef](#)]
14. Mahajan, S. Critique of mechanisms of formation of deformation, annealing and growth twins: Face-centered cubic metals and alloys. *Scr. Mater.* **2013**, *68*, 95–99. [[CrossRef](#)]
15. Zhang, Y.-Q.; Quan, G.-Z.; Zhao, J.; Xiong, W. Influencing mechanisms of prior cold deformation on mixed grain boundary network in the thermal deformation of Ni80A superalloy. *Materials* **2022**, *15*, 6426. [[CrossRef](#)] [[PubMed](#)]
16. Tikhonova, M.; Kuzminova, Y.; Fang, X.; Wang, W.; Kaibyshev, R.; Belyakov, A.  $\Sigma 3$  CSL boundary distributions in an austenitic stainless steel subjected to multidirectional forging followed by annealing. *Philos. Mag.* **2014**, *94*, 4181–4196. [[CrossRef](#)]

17. Odnobokova, M.; Tikhonova, M.; Belyakov, A.; Kaibyshev, R. Development of  $\Sigma 3^n$  CSL boundaries in austenitic stainless steels subjected to large strain deformation and annealing. *J. Mater. Sci.* **2017**, *52*, 4210–4223. [[CrossRef](#)]
18. Pande, C.S.; Imam, M.A. Grain growth and twin formation in boron-doped nickel polycrystals. *Mater. Sci. Eng. A* **2009**, *A512*, 82–86. [[CrossRef](#)]
19. Jin, Y.; Lin, B.; Bernacki, M.; Rohrer, G.S.; Rollet, A.D.; Bozzolo, N. Thermo-mechanical factors influencing annealing twin development in nickel during recrystallization. *Mater. Sci. Eng. A* **2014**, *A597*, 295–303. [[CrossRef](#)]
20. Fang, X.; Liu, Z.; Tikhonova, M.; Belyakov, A.; Wang, W. Evolution of texture and development of  $\Sigma 3^n$  grain clusters in 316 austenitic stainless steel during thermal mechanical processing. *J. Mater. Sci.* **2013**, *48*, 997–1004. [[CrossRef](#)]
21. Humphreys, F.J.; Hatherly, M. *Recrystallization and Related Annealing Phenomena*; Elsevier Science: New York, NY, USA, 2004.
22. Frost, H.J.; Ashby, M.F. *Deformation Mechanism Maps*; Pergamon Press: Oxford, UK, 1982.
23. Sakai, T. Dynamic recrystallization microstructures under hot working conditions. *J. Mater. Proc. Technol.* **1995**, *53*, 349–361. [[CrossRef](#)]
24. Chen, Z.; Chen, Y. Nanocrystalline gradient engineering: Grain evolution and grain boundary networks. *Comp. Mater. Sci.* **2018**, *141*, 282–292. [[CrossRef](#)]
25. Czubyko, U.; Sursaeva, V.G.; Gottstein, G.; Shvindlerman, L.S. Influence of triple junctions on grain boundary motion. *Acta Mater.* **1998**, *46*, 5863–5871. [[CrossRef](#)]